ChemComm

COMMUNICATION

View Article Online
View Journal | View Issue

Cite this: *Chem. Commun.*, 2018, **54**, 8637

Received 27th April 2018,
Accepted 10th July 2018

DOI: 10.1039/c8cc03446j

rsc.li/chemcomm

Structural differences between toxic and nontoxic HypF-N oligomers†

Claudia Capitini,[a] Jayneil R. Patel,[b] Antonino Natalello,[c] Cristiano D'Andrea,[d] Annalisa Relini,[e] James A. Jarvis,[b] Leila Birolo,[f] Alessia Peduzzo,[a] Michele Vendruscolo,[g] Paolo Matteini,[d] Christopher M. Dobson,[g] Alfonso De Simone[b] and Fabrizio Chiti*[a]

We have studied two misfolded oligomeric forms of the protein HypF-N, which show similar morphologies but very different toxicities. We measured over 80 intermolecular distance-dependent parameters for each oligomer type using FRET, in conjunction with solution- and solid-state NMR and other biophysical techniques. The results indicate that the formation of a highly organised hydrogen bonded core in the toxic oligomers results in the exposure of a larger number of hydrophobic residues than in the nontoxic species, causing the former to form aberrant interactions with cellular components.

In the majority of neurodegenerative diseases arising from protein misfolding and deposition, the primary pathogenic agents appear to be the small oligomeric species that are generated as on- or off-pathway intermediate assemblies during fibril formation, or are released by mature fibrils, or form as a consequence of secondary nucleation on the surface of preformed fibrils.[1–4] The small size and presence of solvent-exposed hydrophobic residues on the surfaces of the misfolded oligomers are likely to be key structural elements resulting in their ability to interact aberrantly with cellular components, such as proteins or biological membranes.[1,5–11]

Studies of the N-terminal domain of the *E. coli* protein HypF (HypF-N) have contributed significantly to our knowledge of the structure-toxicity relationship of protein misfolded oligomers.[6,9,12–14] Protocols have been established to form two stable forms of HypF-N oligomers, denoted 'toxic' (type A) and 'nontoxic' (type B), both having a stability sufficient to allow their detailed study with structural and biological techniques.[9,12–14] Here we have characterised both types of HypF-N oligomers in residue-specific structural detail by using a number of biophysical techniques, including solution-state and solid-state NMR spectroscopy, as well as site-directed fluorophore-labelling coupled with FRET measurements to probe over 80 intermolecular distances between different residues in the sequence, with the aim of identifying the specific structural elements responsible for their different toxicities. We first verified that the two oligomeric species could be formed with the same morphological and structural characteristics as those observed previously.[9] AFM images, FTIR and Raman spectroscopic data revealed a spherical bead-like morphology, and a predominance of β-sheet secondary structure (Fig. S1A–C and S2, ESI†). Moreover, both types of oligomers bind ThT and increase its fluorescence by *ca.* 6.5 and 4 fold for type A and B oligomers, respectively (Fig. S1D, ESI†). These observations are in a very good agreement with those found previously.[9] The difference in ThT binding suggests that the β-sheet structure is more organised and compact in type A oligomers than type B.

^{13}C–^{13}C dipolar-assisted rotational resonance (DARR) correlation spectra, obtained using magic angle spinning (MAS) solid-state NMR, were measured for both types of oligomers to detect correlations between carbon atoms in highly rigid regions.[15] ^{13}C–^{13}C DARR is a homonuclear dipolar recoupling experiment, which generates correlations between both backbone and side chain ^{13}C resonances in the protein.[15] ^{13}C–^{13}C DARR spectra obtained with a mixing time of 20 ms (Fig. 1A), as well as ^{13}C–^{15}N correlation spectra (Fig. S3, ESI†), show significant inhomogeneous line broadening attributable to the structural heterogeneity of the samples that precluded sequential assignment of the core regions of the oligomers. However, the high degree of overlap in the ^{13}C–^{13}C DARR resonances of the two types of oligomers indicates that their core regions are structurally similar, with chemical shift ranges showing a high content of

[a] *Department of Experimental and Clinical Biomedical Sciences, University of Florence, Viale Morgagni 50, 50134 Firenze, Italy. E-mail: fabrizio.chiti@unifi.it*
[b] *Department of Life Sciences, Imperial College London, South Kensington, SW72AZ London, UK*
[c] *Department of Biotechnology and Biosciences, University of Milano-Bicocca, Piazza della Scienza 2, 20126 Milano, Italy*
[d] *Institute of Applied Physics, National Research Council, Via Madonna del Piano 10, 50019 Sesto Fiorentino, Italy*
[e] *Department of Chemistry and Industrial Chemistry, University of Genoa, Via Dodecaneso 31, 16146, Genova, Italy*
[f] *Department of Chemical Sciences, University of Naples "Federico II", Monte S. Angelo Campus, Via Cinthia, 80126, Napoli, Italy*
[g] *Centre for Misfolding Diseases, Department of Chemistry, University of Cambridge, Lensfield Road, Cambridge CB2 1EW, UK*

† Electronic supplementary information (ESI) available. See DOI: 10.1039/c8cc03446j

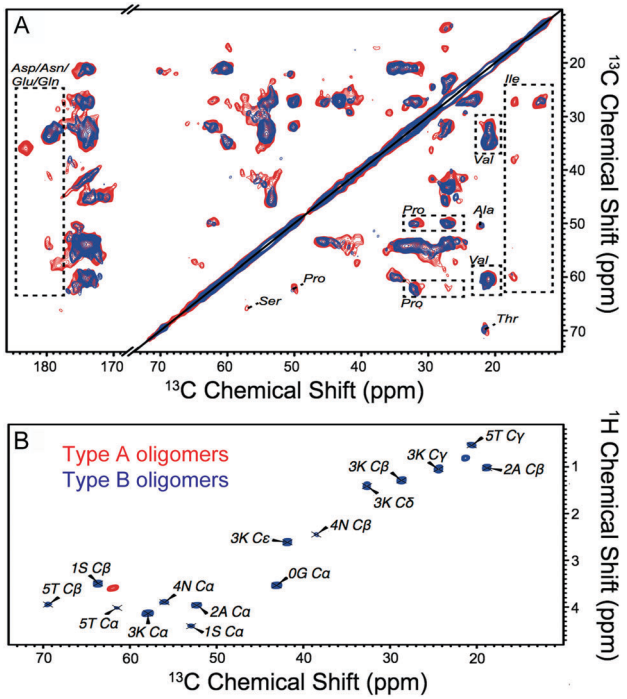

Fig. 1 ssNMR spectra of type A (red) and type B (blue) HypF-N oligomers. (A) ^{13}C–^{13}C-DARR spectra recorded with a 20 ms mixing time. (B) ^{1}H–^{13}C INEPT correlation spectra.

β-sheet structure in both oligomers. Nevertheless, additional resonances were specifically detected in the ^{13}C–^{13}C DARR spectrum of type A oligomers (Fig. 1A and Fig. S3, ESI†), suggesting that their core possesses a greater degree of structural rigidity. In particular, the ^{13}C–^{13}C DARR spectrum of type A oligomers revealed unique cross-correlation peaks between chemical groups from various residue types, including serine (Cα–Cβ), proline (Cβ–Cγ), and isoleucine (Cα–Cγ2, Cβ–Cγ2, Cγ1–Cγ2) residues (Fig. 1A).

^{1}H–^{13}C insensitive nuclei enhanced by polarization transfer (INEPT) experiments, in conjunction with MAS solid-state NMR probed the highly dynamical regions of the two oligomeric forms. Only a single peak is visible in the spectrum of type A oligomers, indicating the absence of regions with a significant dynamical behaviour. Instead, 16 peaks are visible in the spectrum of type B oligomers (Fig. 1B), all assigned to C–H groups of residues 0–5, indicating the presence of protein segments having significant structural mobility.

To obtain information about the solvent-exposure of the various regions of the HypF-N sequence, 12 protein variants carrying a single cysteine residue were produced, labelled with 1,5-IAEDANS, and allowed to form type A and type B oligomers using a 1 : 1 molar ratio of labelled variant to unlabelled wt protein. Although the aggregation kinetics could change after labelling, the 12 forms of type A and type B oligomers were found to bind ThT similarly to those formed by the wt protein (Fig. S4A–C, ESI†). The analysis of the maximum fluorescence of 1,5-IAEDANS (λ_{max}) reveals that the three major hydrophobic regions of the HypF-N sequence are structured in both types of oligomers, but to a lesser extent in type A (Fig. S4D, E, G, ESI† and Fig. 2A). The similarity between the 1,5-IAEDANS λ_{max} profiles and those obtained previously with the pyrene maleimide (PM) excimer ratio[9] (Fig. S4F and G, ESI†), where PM is a more hydrophobic probe than 1,5-IAEDANS, is remarkable as it indicates that the aggregation process of HypF-N under both conditions is not affected by the degree of hydrophobicity of the probe used to label the oligomers and that the labelling does not alter significantly the structure and physicochemical properties of the aggregates. The combined analysis using 1,5-IAEDANS-labelling in the present work and PM-labelling[9] indicates that the three major regions of the sequence that are highly structured in both oligomers, particularly type B, encompass residues 18–30, 55–65 and 75–87, whereas the remainder of the sequence is more flexible (Fig. 2A).

The three-dimensional structures of the two oligomer types were then probed using FRET, by determining the intermolecular interactions between pairs of residues labelled with 1,5-IAEDANS, used as the donor, and 6-IAF as the acceptor, located in different molecules and at different positions in the polypeptide chain. The designation '*x*D_*y*A' indicates oligomers labelled with the donor and acceptor at residue *x* and *y*, respectively (for example 65D_5A indicates oligomers with the donor and acceptor at positions 65 and 5, respectively). A first control experiment, where the HypF-N variant with the cysteine at position 65 was labelled separately with donor and acceptor and mixed together in a 1 : 1 molar ratio maintaining their monomeric folded state, confirmed the expected absence of FRET (Fig. S5, ESI†). A series of experiments was then carried out by incubating the donor- and acceptor-labelled HypF-N variants in a 1 : 1 molar ratio, under the two conditions A and B. We were able to analyse the spectra from a total of 98 *x*D_*y*A type A (Fig. S6, ESI†) and 79 *x*D_*y*A type B (Fig. S7, ESI†) oligomers. In this analysis we excluded all pairs where the donor and acceptor were located on the same hydrophobic regions, as their close intermolecular contact[9] is expected to introduce steric hindrance with perturbations to the oligomer structures. In addition to the oligomers *x*D_*y*A, the oligomers *x*D_wt (where the variant with the acceptor is replaced by the unlabelled wt) and wt_*y*A (where the variant with the donor is replaced by the unlabelled wt) were also produced, since the resulting spectra were necessary for the determination of the FRET efficiency (*E*) value, as described in Fig. S8 (ESI†). Fig. 2B shows the spectra of *x*D_*y*A, *x*D_wt and wt_*y*A obtained for 2 representative type A (left) and type B (right) oligomers. Partial FRET was observed in all cases, and the spectrum of a given oligomeric sample *x*D_*y*A (blue spectra) is characterized by a lower fluorescence emission of the donor compared to the spectrum *x*D_wt (red spectra), and a higher fluorescence emission of the acceptor compared to the spectrum wt_*y*A (green spectra) for all the cases reported (Fig. 2B and Fig. S6, S7, ESI†). The *E* values calculated for all the type A and B labelled oligomers are reported in Fig. S9 (ESI†).

To interpret fully the calculated *E* values, in each case the difference between the values determined for the type A (E_A) and type B (E_B) oligomers, that is $\Delta E = E_A - E_B$, was calculated (Fig. 2C). The first observation is that the *E* values measured for the 5D_*y*A or *x*D_5A pairs are, on average, lower in type B oligomers,

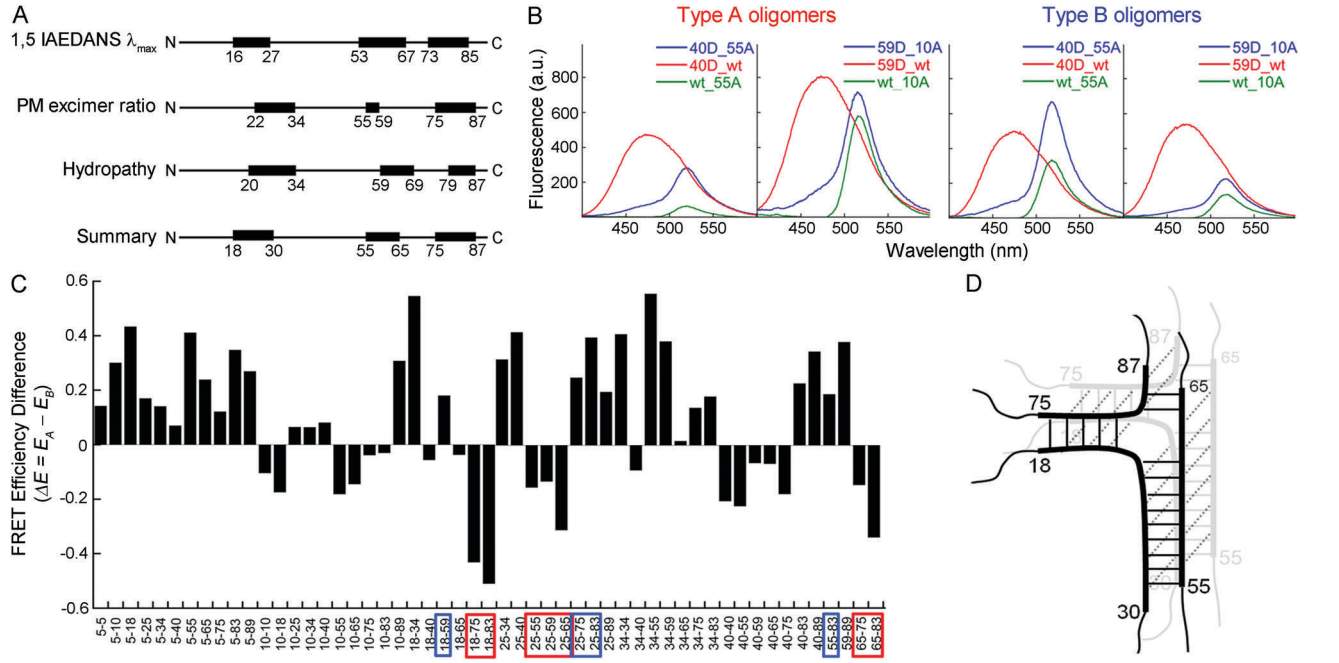

Fig. 2 (A) Scheme of the three regions of the sequence (black bars) that are highly structured in type B and less-well defined in type A HypF-N oligomers, identified by the 1,5-IAEDANS λ_{max} and PM excimer ratio analysis, of the three major hydrophobic regions according to the hydropathy profile, and of the three most structured regions resulting from the three analyses (Summary). (B) Fluorescence emission spectra of samples *x*D_*y*A (blue), *x*D_wt (red), and wt_*y*A (green) after aggregation under conditions A (left) and B (right). The oligomers shown in each panel are 40D_55A and 59D_10A. (C) Differences between the *E* values of type A and type B oligomers ($\Delta E = E_A - E_B$) for the pairs of residues reported on the *x* axis; the pairs in boxes indicate interactions between hydrophobic residues with $\Delta E < 0$ (red) or $\Delta E > 0$ (blue). (D) Schematic representation of the three more highly structured regions of the HypF-N sequence (residues 18–30, 55–65, and 75–87) in the nontoxic type B oligomers. The intermolecular interactions both involve homologous regions in neighbouring molecules (oblique lines), as shown previously,[9] and non-homologous regions in neighbouring molecules (horizontal lines).

suggesting that the intermolecular distances between the N-terminus and other portions of the sequence in adjacent protein molecules in the oligomers are longer in the case of type B oligomers. This observation is consistent with the ^{1}H–^{13}C INEPT ssNMR analysis, showing a high degree of flexibility of the N-terminal region in type B oligomers. The second observation is that the *E* values measured for many of the distances between hydrophobic regions are higher in type B oligomers (Fig. S9, ESI† and Fig. 2C red boxes), indicating that the donor and acceptor fluorophores are, on average, closer together. In particular, among all pairs 18D_*y*A, the pairs 18D_75A and 18D_83A have the highest *E* values in the type B oligomers, but these values are much lower in the type A oligomers; among all pairs 25D_*y*A, the pairs 25D_55A, 25D_59A and 25D_65A have the highest *E* values in the type B oligomers, but lower values in the type A; among all the pairs 65D_*y*A, the pairs 65D_75A and 65D_83A have the highest *E* values in the type B oligomers, again with lower values in the type A species. These results imply that the three main hydrophobic regions (regions 18–30, 55–65, 75–87) appear to interact more closely in type B relative to type A oligomers, not just because of closer contacts in the type B oligomers between corresponding regions of the sequence in different molecules (for example between segments 18–30 from different molecules), but also because of weaker interactions between different regions in type A oligomers. Moreover, in the nontoxic type B species, well-defined connectivities are observed to link the N-terminal residues of the region 18–30 and the entire region of residues 75–87, between the C-terminal segment 18–30 and the N-terminal segment of residues 55–65, and between the C-terminal stretch of the region 55–65 and the entire region 75–87 (Fig. 2D). All such interactions appear to be less well-defined in the toxic type A oligomers, as shown by their lower FRET efficiency values, hence increasing the availability of hydrophobic groups for interactions with cellular components.

Limited proteolysis with trypsin, chymotrypsin and proteinase K was then used to investigate the differences in structural accessibility of regions in the two forms of oligomers formed by the wt protein. The samples were analysed by MALDI-TOF mass spectrometry to detect the proteolysed fragments. Some proteolytic sites are evident very early during the proteolytic treatment (after 3 min) for both oligomers, indicating that some regions in both species are highly flexible and exposed (Fig. 3). Interestingly, all the residues close to the N-terminus (R12, R14, K16) are proteolysed only in the type B species, confirming the structural flexibility of this portion of the protein. In addition, W27 in the first hydrophobic region is seen to be proteolysed only in type A oligomers, and Y62, located in the second hydrophobic region, is more susceptible to proteolysis in type A oligomers, as suggested by its vulnerability to two proteases, rather than just one, after 20 min. Interestingly, at all incubation times there are more sites of proteolysis observed for the type B than for the type A oligomers, suggesting a higher overall

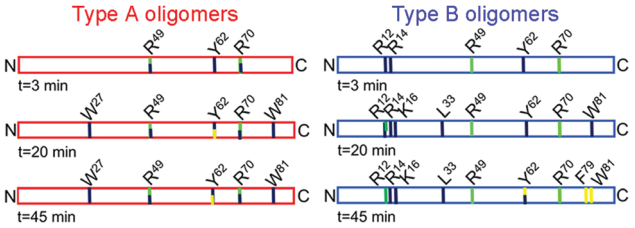

Fig. 3 Cleavage sites observed in type A and type B oligomers of wt HypF-N at different times of exposure to proteolytic conditions. Green, yellow and blue bars indicate cleavage by trypsin, chymotrypsin and proteinase K, respectively. Bars shown with two colours are cleavage sites detected with two enzymes.

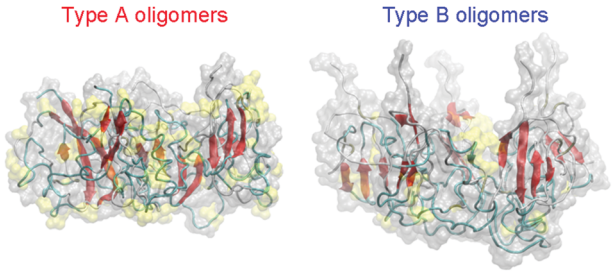

Fig. 4 Schematic representation of toxic type A and nontoxic type B oligomers of HypF-N indicating disordered regions (grey/green), β-strands (red) and hydrophobic side chains (yellow). The two types of oligomers have a similar content of β-sheet structure and overall structure. However, the type A are more rigid, contain a less disordered N-terminal region, and have a higher solvent-exposure of the hydrophobic residues.

flexibility of the protein molecules in the former, if we include the N-terminal segment (Fig. 3). Such a difference is not observed in locations other than the N-terminal region, again a result consistent with the ^{1}H–^{13}C INEPT NMR and FRET analyses.

Finally, the mechanism of formation of the two types of oligomers at the individual residue level was investigated by performing chemical exchange saturation transfer (CEST) experiments in solution state ^{15}N–^{1}H-HSQC spectra (Fig. S10, ESI†). The CEST experiments can identify the residues that are strongly associated with the slow-tumbling core of the oligomers, *i.e.*, which exhibit high saturation levels at the various frequency offsets employed here (*i.e.* having low I/I_0 ratios) and therefore indicate the regions involved in the first contacts in the process of oligomerisation (Fig. S10, ESI†). A related approach, using CPMG based relaxation dispersion solution NMR experiments, has been used to study $A\beta_{40}$.[16]

In conclusion, the toxic and nontoxic HypF-N oligomers appear to have a similar morphology, to bind ThT weakly but significantly, and to have a similar core structure based on a β-sheet scaffold (Fig. 4). However, by monitoring NMR resonances in solution and in the solid-state, and measuring more than 80 intermolecular interactions by quantitative FRET measurements in both oligomer types, we have identified important structural characteristics that distinguish the toxic type A from the nontoxic type B oligomers, involving in the first case a higher overall degree of compactness and a lower persistence of well-defined intermolecular hydrophobic interactions, which involve those between both homologous and non-homologous regions of the sequence (Fig. 4). The combination of these two structural characteristics indicates that the higher overall flexibility of the nontoxic oligomers allows the hydrophobic residues of the protein to form a more compact hydrophobic core, such that the majority of the hydrophobic residues are highly buried in the interior. By contrast, the formation of a more rigid and compact structure in the toxic oligomers generates structural constraints that cause a number of the hydrophobic residues to interact less strongly with each other, such that a fraction of these residues is exposed to the solvent to a sufficient extent to enable aberrant intermolecular interactions with cellular components.

Conflicts of interest

There are no conflicts to declare.

Notes and references

1 F. Chiti and C. M. Dobson, *Annu. Rev. Biochem.*, 2017, **86**, 27.
2 C. A. Lasagna-Reeves, C. G. Glabe and R. Kayed, *J. Biol. Chem.*, 2011, **286**, 22122.
3 I. C. Martins, I. Kuperstein, H. Wilkinson, E. Maes, M. Vanbrabant, W. Jonckheere, P. Van Gelder, D. Hartmann, R. D'Hooge, B. De Strooper, J. Schymkowitx and F. Rousseau, *EMBO J.*, 2008, **27**, 224.
4 G. Meisl, X. Yang, E. Hellstrand, B. Frohm, J. B. Kirkegaard, S. I. Cohen, C. M. Dobson, S. Linse and T. P. Knowles, *Proc. Natl. Acad. Sci. U. S. A.*, 2014, **111**, 9384.
5 J. Ojha, G. Masilamoni, D. Dunlap, R. A. Udoff and A. G. Cashikar, *Mol. Cell. Biol.*, 2011, **31**, 3146.
6 B. Mannini, R. Cascella, M. Zampagni, M. van Waarde-Verhagen, S. Meehan, C. Roodveldt, S. Campioni, M. Boninsegna, A. Penco, A. Relini, H. H. Kampinga, C. M. Dobson, M. R. Wilson, C. Cecchi and F. Chiti, *Proc. Natl. Acad. Sci. U. S. A.*, 2012, **109**, 12479.
7 R. Cascella, S. Conti, B. Mannini, X. Li, J. N. Buxbaum, B. Tiribilli, F. Chiti and C. Cecchi, *Biochim. Biophys. Acta*, 2013, **1832**, 2302.
8 B. Bolognesi, J. R. Kumita, T. P. Barros, E. K. Esbjorner, L. M. Luheshi, D. C. Crowther, M. R. Wilson, C. M. Dobson, G. Favrin and J. J. Yerbury, *ACS Chem. Biol.*, 2010, **5**, 735.
9 S. Campioni, B. Mannini, M. Zampagni, A. Pensalfini, C. Parrini, E. Evangelisti, A. Relini, M. Stefani, C. M. Dobson, C. Cecchi and F. Chiti, *Nat. Chem. Biol.*, 2010, **6**, 140.
10 A. R. Ladiwala, J. Litt, R. S. Kane, D. S. Aucoin, S. O. Smith, S. Ranjan, J. Davis, W. E. Vannostrand and P. M. Tessier, *J. Biol. Chem.*, 2012, **287**, 24765.
11 R. Krishnan, J. L. Goodman, S. Mukhopadhyay, C. D. Pacheco, E. A. Lemke, A. A. Deniz and S. Lindquist, *Proc. Natl. Acad. Sci. U. S. A.*, 2012, **109**, 11172.
12 M. Zampagni, R. Cascella, F. Casamenti, C. Grossi, E. Evangelisti, D. Wright, M. Becatti, G. Liguri, B. Mannini, S. Campioni, F. Chiti and C. Cecchi, *J. Cell. Mol. Med.*, 2011, **15**, 2106.
13 F. Tatini, A. M. Pugliese, C. Traini, S. Niccoli, G. Maraula, T. Ed Dami, B. Mannini, T. Scartabelli, F. Pedata, F. Casamenti and F. Chiti, *Neurobiol. Aging*, 2013, **34**, 2100.
14 B. Mannini, E. Mulvihill, C. Sgromo, R. Cascella, R. Khodarahmi, M. Ramazzotti, C. M. Dobson, C. Cecchi and F. Chiti, *ACS Chem. Biol.*, 2014, **9**, 2309.
15 K. Takegoshi and T. Terao, *Solid State Nucl. Magn. Reson.*, 1999, **13**, 203.
16 J. Krishnamoorthy, J. R. Brender, S. Vivekanandan, N. Jahr and A. Ramamoorthy, *J. Phys. Chem. B*, 2012, **116**, 13618.

